Charge Detection Using a van der Waals Heterostructure Based on Monolayer WSe_2

Justin Boddison-Chouinard,[1] Alex Bogan,[2] Norman Fong,[3] Pedro Barrios,[3] Jean Lapointe,[3] Kenji Watanabe,[4] Takashi Taniguchi,[4] Adina Luican-Mayer,[1,*] and Louis Gaudreau[2,†]

[1] *Department of Physics, University of Ottawa, Ottawa, Ontario K1N 9A7, Canada*

[2] *Emerging Technologies Division, National Research Council of Canada, Ottawa, Ontario K1A 0R6, Canada*

[3] *Advanced Electronics and Photonics, National Research Council of Canada, Ottawa, Ontario K1A 0R6, Canada*

[4] *International Center for Materials Nanoarchitectonics, National Institute for Materials Science, 1-1 Namiki, Tsukuba 305-0044, Japan*

(Received 18 May 2022; revised 14 September 2022; accepted 19 September 2022; published 7 November 2022)

Charge detection is a crucial component used in semiconductor quantum circuits. It allows the non-invasive readout of charge and spin qubits in quantum information protocols and can also be leveraged for quantum sensing applications. In this work, we demonstrate that van der Waals heterostructure devices with gated nanoconstrictions in monolayer WSe_2 can be used as charge detectors for nearby quantum dots. This is a demonstration of charge detection using transition-metal dichalcogenides, and we find that the detection sensitivity is comparable to that of other two-dimensional (2D) material charge detectors based on graphene. These results open the possibility of implementing charge detection schemes based on 2D materials in complex quantum circuits.

DOI: 10.1103/PhysRevApplied.18.054017

I. INTRODUCTION

The detection and manipulation of individual charges and spins is at the heart of developing quantum technologies. In particular, the detection of individual charges in a quantum dot (QD) can be realized by placing a quantum point contact (QPC) in its vicinity and detecting changes in the conductance through the QPC current as a result of the altered electrostatic environment around the QD. While transport directly through a single quantum dot and charged detection are equivalent, this is not the case for circuits containing more than a single quantum dot. In that situation direct transport only occurs under specific resonance conditions between dots, which becomes severely restrictive as additional quantum dots are added. This is in contrast to charge detection techniques that are able to identify the charge in each dot separately without current flowing directly through the circuit. As a result, charge detection technology is a requirement for complex spin qubit quantum circuits [1–3]. The implementation of this approach was initially successfully demonstrated in GaAs two-dimensional (2D) electron gas devices [4]. More recently, 2D materials including graphene and semiconducting transition-metal dichalcogenides (TMDs) have emerged as a novel platform to realize electrostatically confined quantum circuits. Within the 2D materials platform, QPCs have been demonstrated in TMDs [5–10], and more specifically, QPC charge detection has been demonstrated in monolayer and bilayer graphene (BLG) devices [11–16]. However, charge detection has not yet been implemented in semiconducting TMDs. The direct band gap in TMDs, along with the interplay of the spin and valley degrees of freedom, makes them an appealing platform for realizing hybrid quantum circuits with optical and solid-state qubits [17–19]. Additionally, the strong spin-orbit coupling in TMDs could enable fast spin qubit manipulation with ac electric fields [20] and lead to spin-valley locking, by which qubits could be more robust against electromagnetic noise. Although gated quantum dots in TMDs have been recently realized [5,6,8,21–23], charge detection using gated nanoconstrictions is yet to be implemented. In this work, we realize a nanoconstriction in a monolayer (ML) WSe_2 channel and demonstrate charge detection of a gate-controlled WSe_2 quantum dot.

II. SAMPLE FABRICATION

The charge detector device used in this work is based on monolayer WSe_2, schematically described in Fig. 1(a). Its optical micrograph is shown in Fig. 1(b). The device is assembled on a p-Si/SiO_2 (285 nm) substrate using standard dry transfer methods. Local control gates [Ti(2.5

*luican-mayer@uottawa.ca

†Louis.Gaudreau@nrc-cnrc.gc.ca

nm)/Au(2.5 nm)] are first deposited on the substrate using electron beam lithography [Fig. 1(b) inset]. They are 100 nm in width, with a lateral spacing of 50 nm, and varying gap spacing (50, 100, and 75 nm). The local control gates are responsible for locally depleting the carriers in the monolayer WSe_2 flake. A flake of hexagonal boron nitride (*h*-BN) of 44 nm in thickness is transferred on top of the prepatterned gates and electrical contacts [Cr(2 nm)/Pt(8 nm)] are subsequently lithographically patterned on top of the *h*-BN. To increase sample cleanliness and, consequently, reduce contact resistance, the device is cleaned in a vacuum furnace (10^{-7} Torr) at 300 °C for 30 min. Additionally, remaining polymer residues are removed using an atomic force microscope (AFM) tip in contact mode [23–25]. A WSe_2 monolayer and a 37-nm-thick *h*-BN flake are exfoliated and identified on independent substrates. Using dry transfer techniques, the *h*-BN flake is first picked up and then used to pick up the WSe_2 flake; subsequently, the WSe_2/*h*-BN stack is precisely placed on top of the cleaned electrical contacts. We note that prior to the deposition of the *h*-BN/WSe_2 stack, the WSe_2 surface is also mechanically cleaned using an AFM tip. A last lithographic step is performed to deposit a top gate [Ti(5 nm)/Pd(20 nm)/Au(100 nm)] used to globally modify the charge carrier density of the WSe_2 flake and to achieve Ohmic contacts.

III. RESULTS AND DISCUSSION

In a first measurement step, the source-drain current is monitored as a function of the top gate voltage (V_{TG}) at a temperature of $T = 4$ K as shown in Fig. 1(c). The current increases at higher negative values of V_{TG}, indicating hole conduction across the WSe_2 channel. At top gate voltage values below −6 V, the current-voltage characteristics across the source-drain contacts show a linear behavior, as presented for select values of V_{TG} in the inset of Fig. 1(c). One of the principal challenges in developing quantum devices in 2D semiconductors is realizing good electrical contacts. Thus, when the temperature is further reduced ($T = 1.5$ K), by using a three-terminal measurement scheme, the contact resistances of the source and drain are individually measured as a function of V_{TG} as seen in Fig. 1(d). The importance of the top gate for achieving high-quality contacts is evidenced by the low contact resistance measured when $V_{TG} = -10$ V. At this top-gate voltage, a contact resistance of 404 Ω is measured for the source contact and 1240 Ω for the drain contact.

We then investigate the influence of the local control gates on the transport properties of the device in a dilution refrigerator with a base temperature below 10 mK. Specifically, the pair of gates $V_{G_{3L}}$ and $V_{G_{3U}}$ [rightmost control gates in the inset of Fig. 1(b)] are studied while

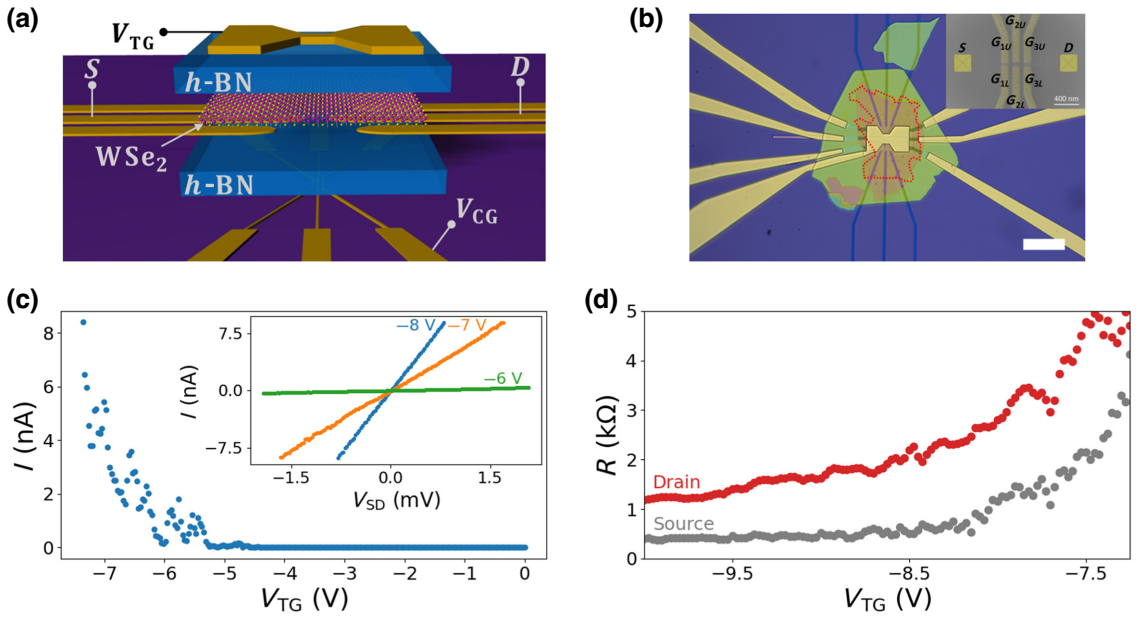

FIG. 1. (a) Schematic architecture of the charge detection device based on monolayer WSe_2. (b) Optical micrograph of the completed device used in this work. The WSe_2 flake is outlined in red for clarity. Scale bar: 20 μm. Inset: false-color scanning electron micrograph of the control gates. (c) Source-drain current as a function of the top gate voltage (V_{TG}) showing the activation curve of the device. Inset: linear *I*-*V* characteristic observed when $V_{TG} < -6$ V. The temperature of these measurements is $T = 4$ K. (d) Contact resistance of the source and drain contacts as a function of the top gate voltage V_{TG}, as indicated. The gray (red) curve represents the resistance associated with the source (drain) contact. The temperature of these measurements is $T = 1.5$ K.

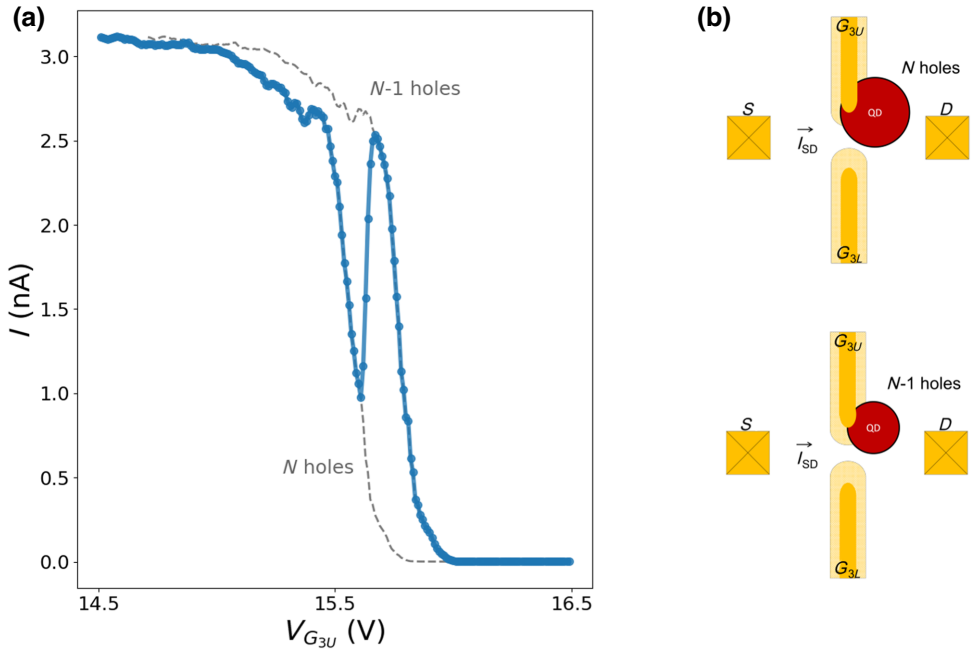

FIG. 2. (a) The blue dotted curve is the source-drain current as a function of the local control gate G_{3U}, while the local control gate $G_{3L} = 15.12$ V. The gray dashed curves are guides for two distinct quantum dot populations N and $N - 1$, as indicated. (b) Schematic explanation of the result observed in (a), where a change in the hole population of a nearby quantum dot affects the channel width and the source-drain current. $T < 10$ mK.

all other control gates are grounded (Fig. 2). A bias voltage of 500 μV is applied to the source contact, while the drain contact is grounded. A gradually increasing voltage is applied to both $V_{G_{3L}}$ and $V_{G_{3U}}$ to create a channel by locally depleting the WSe_2 flake of holes in the areas directly above the two control gates. Keeping $V_{G_{3L}}$ at 15.12 V, $V_{G_{3U}}$ is varied, while the source-drain current I is monitored, as shown in Fig. 2(a) (blue dotted curve). The source-drain current decreases as a function of $V_{G_{3U}}$ until $V_{G_{3U}} = 15.6$ V, when it suddenly increases, and, as $V_{G_{3U}}$ is further increased, the current eventually pinches off. We demonstrate below that this is related to the nanoconstriction acting as a noninvasive probe of the charge of a nearby incidental quantum dot formed by the potential landscape created by impurities and defects in the environment around the WSe_2 layer [23,26].

Figure 2(b) illustrates the model for the blue current trace characteristics observed in Fig. 2(a). A nearby

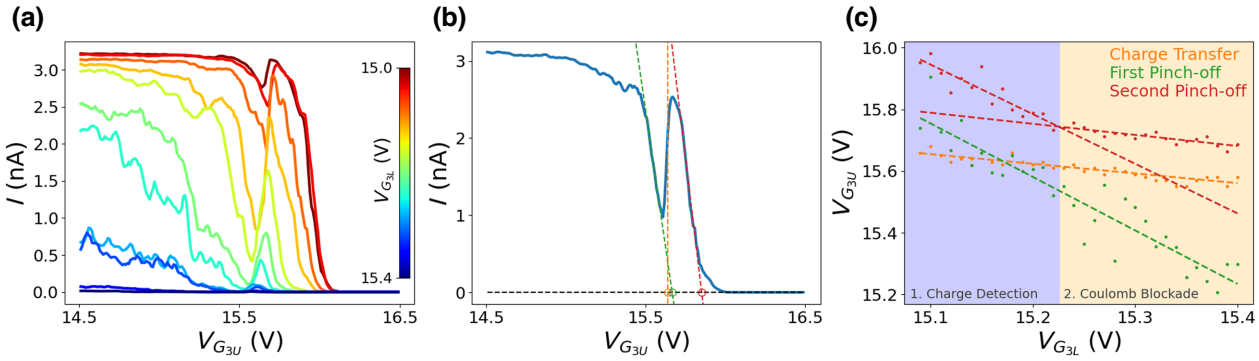

FIG. 3. (a) Source-drain current as a function of the local control gate $V_{G_{3U}}$. Curves are taken for different values of $V_{G_{3L}}$ ranging from 15 V (dark red) to 15.4 V (dark blue). Experimentally, curves are taken at an interval of $\Delta V_{G_{3L}} = 0.01$ V but, for clarity, an interval of $\Delta V_{G_{3L}} = 0.05$ V is shown here. (b) An example of how the "positions" of the first pinch-off (green), the second pinch-off (red), and the charge transfer step (orange) are obtained. The trace is taken when the voltage on $V_{G_{3L}} = 15.12$ V. (c) The position of the first pinch-off (green), the second pinch-off (red), and the charge transfer step (orange) plotted as a function of $V_{G_{3L}}$ along with fitted linear regression. $T < 10$ mK.

quantum dot has an initial population of N holes. As a larger positive voltage is applied to the local control gate $V_{G_{3U}}$, the width of the channel formed between $V_{G_{3U}}$ and $V_{G_{3L}}$ decreases, resulting in a decrease of current. At the same time, $V_{G_{3U}}$ controls the chemical potential of the nearby quantum dot and can therefore remove holes from it by applying a larger positive voltage. At a specific gate voltage, the population of the quantum dot transitions from N holes to $N-1$ holes, resulting in a widening of the channel and, as a result, a sudden increase in current through the charge detector.

Assuming no change in the number of holes (N) in the quantum dot as a function of gate voltage, the current is expected to follow the leftmost gray dashed curve in Fig. 2(a). If a hole is removed from the quantum dot, which would be therefore populated by $N-1$ holes, a larger voltage applied to $V_{G_{3U}}$ would be needed to achieve the same result (rightmost gray dashed curve). Thus, the jump between the two gray curves indicates a switch between a nearby quantum dot population of N and $N-1$ holes.

To demonstrate that the observed step in the source-drain current of Fig. 2 is caused by a change in the charge population of a nearby quantum dot, we study the evolution of the charge detection step as a function of $V_{G_{3U}}$ for different values of $V_{G_{3L}}$ between 15 V (dark red curve) and 15.4 V (dark blue curve) as shown in Fig. 3(a). We observe that as $V_{G_{3L}}$ increases, the constriction pinch-off voltage decreases as a function of $V_{G_{3U}}$, while the voltage at which the charge transfer step occurs remains mostly constant. This indicates that the origin of the step is distinct from the nanoconstriction. In addition, we note that a current peak is still visible, but with considerably less amplitude, after the detector is pinched off for higher $V_{G_{3L}}$ values. We attribute this behavior to resonant tunneling through a single energy level in the nearby quantum dot in the Coulomb blockade regime.

To investigate this further, we extract the position of three distinct events in each current trace of Fig. 3(a): the first pinch-off, the second pinch-off, and the charge transfer step. The first pinch-off point is extracted by taking a linear regression of the initial downward slope of the current and obtaining its x intercept. It represents the point in gate voltage where the current would be zero if there is no change in the hole occupation of the nearby quantum dot. Similarly, the second pinch-off point is the x intercept of the linear regression of the current's second downward slope, which occurs because a hole has been ejected from the nearby quantum dot. The charge transfer step is taken to be the middle point between the current's local minimum and local maximum around the step. This represents the gate voltage at which the chemical potential of the quantum dot lies exactly at the midpoint between the source and drain leads. An example of this is illustrated in Fig. 3(b). This analysis is performed for all values of $V_{G_{3L}}$ and plotted in Fig. 3(c). The slopes associated with the first pinch-off point and the charge transfer step are each constant as a function of $V_{G_{3L}}$ and have values of $(-1.7 \pm 0.1)V_{G_{3U}}/V_{G_{3L}}$ and $(-0.34 \pm 0.03)V_{G_{3U}}/V_{G_{3L}}$, respectively. The difference in slopes between the linear dependencies of these events (first pinch-off and charge transfer) further indicates that the origins of the charge transfer step and the nanoconstriction are independent. Looking at the extrapolations associated with the second pinch-off point, we observe a change in slope at $V_{G_{3L}} = 15.22$ V, the voltage where the charge transfer step transitions into a Coulomb blockade peak, associated with resonant tunneling through the quantum dot. The slope corresponding to the second pinch-off point in the charge detection regime $[(-1.6 \pm 0.2)V_{G_{3U}}/V_{G_{3L}}]$ is similar to the slope associated with the first pinch-off point, suggesting its origin being the nanoconstriction. However, in the Coulomb blockade regime, the slope corresponding to second pinch-off $[(-0.35 \pm 0.05)V_{G_{3U}}/V_{G_{3L}}]$ no longer follows the first pinch-off, but instead it follows the charge transfer step. This is due to the fact that at $V_{G_{3L}} > 15.22$ V the constriction is completely pinched off and we are measuring only resonant tunneling through the quantum dot. We note that the quantum dot transport is still present in the charge detection regime; however, the signal is dominated by the transport through the nanoconstriction.

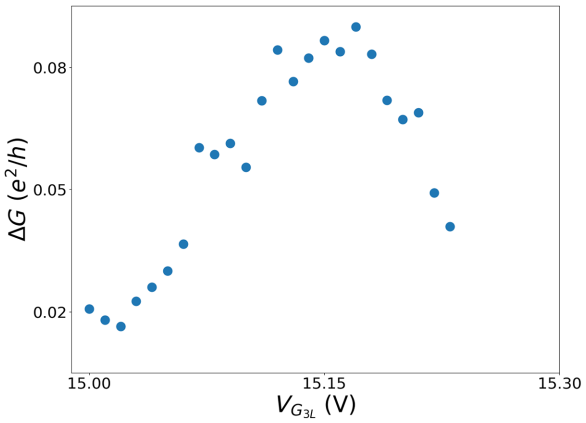

FIG. 4. The charge detection sensitivity (ΔG) of the measured device as a function of the voltage applied to G_{3U}.

The sensitivity of the charge detector, defined as the change of conductance through the nanoconstriction caused by the addition or subtraction of a single hole in the nearby quantum dot in units of e^2/h, is tuned as a function of the voltage applied to $V_{G_{3L}}$ as can be seen in Fig. 4. An optimal value of $0.09e^2/h$ is reached when $V_{G_{3L}} = 15.17$ V. At this point, the derivative of the current with respect to the gate voltage, $dI/dV_{G_{3L}}$, is maximum, indicating that the sensitivity of the constriction to its electrostatic environment is highest. Table I compares this sensitivity with those of previously reported charge detectors using

TABLE I. Comparison of the charge detector sensitivity (ΔG) for various 2D material devices.

Reference	ΔG (e^2/h)	Material
Appl. Phys. Lett. (2008) [11]	10^{-4}	Graphene
Appl. Phys. Lett. (2010) [12]	< 0.1	Graphene
Phys. Status Solidi B (2011) [15]	0.005	BLG
Phys. Rev. B (2011) [13]	0.02	Graphene
Nat. Commun. (2013) [14]	0.002	Graphene
Nano Lett. (2019) [16]	0.2	BLG
This work (2022)	0.09	ML WSe_2

graphene and bilayer graphene devices (dot-detector distances range from 35 to 150 nm), suggesting that TMDs show promising prospects of being used in charge detection schemes based on nanoconstrictions. We note that the high sensitivity of the TMD device in this work can be partially attributed to the close proximity of the incidental quantum dot to the detector.

IV. CONCLUSION

In summary, we fabricate van der Waals heterostructure devices where we electrostatically define nanoconstrictions in monolayer WSe_2. Our fabrication technique results in very low contact resistance, which allows the study of transport properties through the constrictions. By monitoring the current in a nanoconstriction, we demonstrate using a TMD (monolayer WSe_2) the possibility of using such a device as a charge sensor for nearby quantum dots. The sensitivity of the WSe_2 is comparable to that similar devices implemented in graphene and bilayer graphene. Further material and device optimization is required to realize more tunable quantum circuits with highly sensitive charge detection using TMDs. These results pave the way for future development of complex quantum circuits, where charge detectors can be integrated into gated quantum dot architectures.

ACKNOWLEDGMENTS

We would like to thank Dr. Andrew Sachrajda for fruitful discussions. This work is supported by the High Throughput and Secure Networks Challenge Program at the National Research Council of Canada. A.L.-M. and J.B.-C. acknowledge funding from National Sciences and Engineering Research Council (NSERC) Discovery Grant No. RGPIN-2016-06717. We also acknowledge the support of the Natural Sciences and Engineering Research Council of Canada (NSERC) through Strategic Project STPGP 521420. K.W. and T.T. acknowledge support from JSPS KAKENHI (Grants No. 19H05790, No. 20H00354, and No. 21H05233).

[1] J. K. Elzerman, R. Hanson, L. H. Willems van Beveren, B. Witkamp, L. M. K. Vandersypen, and L. P. Kouwenhoven, Single-shot read-out of an individual electron spin in a quantum dot, Nature **430**, 431 (2004).

[2] J. R. Petta, A. C. Johnson, J. M. Taylor, E. A. Laird, A. Yacoby, M. D. Lukin, C. M. Marcus, M. P. Hanson, and A. C. Gossard, Coherent manipulation of coupled electron spins in semiconductor quantum dots, Science **309**, 2180 (2005).

[3] G. Granger, D. Taubert, C. E. Young, L. Gaudreau, a. Kam, S. a. Studenikin, P. Zawadzki, D. Harbusch, D. Schuh, W. Wegscheider, Z. R. Wasilewski, a. a. Clerk, S. Ludwig, and a. S. Sachrajda, Quantum interference and phonon-mediated back-action in lateral quantum-dot circuits, Nat. Phys. **8**, 522 (2012).

[4] M. Field, C. G. Smith, M. Pepper, D. A. Ritchie, J. E. F. Frost, G. A. C. Jones, and D. G. Hasko, Measurements of Coulomb Blockade with a Noninvasive Voltage Probe, Phys. Rev. Lett **70**, 1311 (1993).

[5] R. Pisoni, Y. Lee, H. Overweg, M. Eich, P. Simonet, K. Watanabe, T. Taniguchi, R. Gorbachev, T. Ihn, and K. Ensslin, Gate-defined one-dimensional channel and broken symmetry states in MoS_2 van der Waals heterostructures, Nano Lett. **17**, 5008 (2017).

[6] Z.-Z. Zhang, X.-X. Song, G. Luo, G.-W. Deng, V. Mosallanejad, T. Taniguchi, K. Watanabe, H.-O. Li, G. Cao, G.-C. Guo, F. Nori, and G.-P. Guo, Electrotunable artificial molecules based on van der Waals heterostructures, Sci. Adv. **3**, e1701699 (2017).

[7] K. Marinov, A. Avsar, K. Watanabe, T. Taniguchi, and A. Kis, Time-resolved charge detection in graphene quantum dots, Nat. Commun. **8**, 1938 (2017).

[8] K. Wang, K. D. Greve, L. A. Jauregui, A. Sushko, A. High, Y. Zhou, G. Scuri, T. Taniguchi, K. Watanabe, M. D. Lukin, H. Park, and P. Kim, Electrical control of charged carriers and excitons in atomically thin materials, Nat. Nanotechnol. **13**, 128 (2018).

[9] A. Epping, L. Banszerus, J. Güttinger, L. Krückeberg, K. Watanabe, T. Taniguchi, F. Hassler, B. Beschoten, and C. Stampfer, Quantum transport through MoS_2 constrictions defined by photodoping, J. Phys.: Condens. Matter **30**, 205001 (2018).

[10] K. Sakanashi, P. Krüger, K. Watanabe, T. Taniguchi, G.-H. Kim, D. K. Ferry, J. P. Bird, and N. Aoki, Signature of spin-resolved quantum point contact in p-type trilayer WSe_2 van der Waals heterostructure, Nano Lett. **21**, 7534 (2021).

[11] J. Güttinger, C. Stampfer, S. Hellmüller, F. Molitor, T. Ihn, and K. Ensslin, Charge detection in graphene quantum dots, Appl. Phys. Lett. **93**, 212102 (2008).

[12] L. Wang, G. Cao, T. Tu, H.-O. Li, C. Zhou, Z. Su, X.-J. Hao, G.-C. Guo, H.-W. Jiang, and G.-P. Guo, A graphene quantum dot with a single electron transistor as an integrated charge sensor, Appl. Phys. Lett. **97**, 262113 (2010).

[13] J. Güttinger, J. Seif, C. Stampfer, A. Capelli, K. Ensslin, and T. Ihn, Time-resolved charge detection in graphene quantum dots, Phys. Rev. B **83**, 165445 (2011).

[14] C. Volk, C. Neumann, S. Fringes, S. Engels, F. Haupt, A. Müller, and C. Stampfer, Probing relaxation times in graphene quantum dots, Nat. Commun. **4**, 1753 (2013).

[15] S. Fringes, C. Volk, C. Norda, B. Terrés, J. Dauber, S. Engels, S. Trellenkamp, and C. Stampfer, Charge detection in a bilayer graphene quantum dot, Phys. Status Solidi B **248**, 2684 (2011).

[16] A. Kurzmann, H. Overweg, M. Eich, A. Pally, P. Rickhaus, R. Pisoni, K. Watanabe, T. Taniguchi, T. Ihn, and K. Ensslin, Charge detection in gate-defined bilayer graphene quantum dots, Nano Lett. **19**, 5216 (2019).

[17] T. Fujita, K. Morimoto, H. Kiyama, G. Allison, M. Larsson, A. Ludwig, S. R. Valentin, A. D. Wieck, A. Oiwa, and S. Tarucha, Angular momentum transfer from photon polarization to an electron spin in a gate-defined quantum dot, Nat. Commun. **10**, 2991 (2019).

[18] H. Kosaka, T. Inagaki, R. Hitomi, F. Izawa, Y. Rikitake, H. Imamura, Y. Mitsumori, and K. Edamatsu, Coherent transfer of time-bin photons to electron spins in a semiconductor, Phys. Rev. A **85**, 042304 (2012).

[19] L. Gaudreau, A. Bogan, M. Korkusinski, S. Studenikin, D. Austing, and A. Sachrajda, Entanglement distribution schemes employing coherent photon-to-spin conversion in semiconductor quantum dot circuits, Semicond. Sci. Technol. **32**, 093001 (2017).

[20] K. C. Nowack, F. H. Koppens, Y. V. Nazarov, and L. M. K. Vandersypen, Coherent control of a single electron spin with electric fields, Science **318**, 1430 (2007).

[21] R. Pisoni, Z. Lei, P. Back, M. Eich, H. Overweg, Y. Lee, K. Watanabe, T. Taniguchi, T. Ihn, and K. Ensslin, Gate-tunable quantum dot in a high quality single layer MoS_2 van der Waals heterostructure, Appl. Phys. Lett. **112**, 123101 (2018).

[22] S. Davari, J. Stacy, A. Mercado, J. Tull, R. Basnet, K. Pandey, K. Watanabe, T. Taniguchi, J. Hu, and H. Churchill, Gate-Defined Accumulation-Mode Quantum Dots in Monolayer and Bilayer WSe_2, Phys. Rev. Appl. **13**, 054058 (2020).

[23] J. Boddison-Chouinard, A. Bogan, N. Fong, K. Watanabe, T. Taniguchi, S. Studenikin, A. Sachrajda, M. Korkusinski, A. Altintas, M. Bieniek, P. Hawrylak, A. Luican-Mayer, and L. Gaudreau, Gate-controlled quantum dots in monolayer WSe_2, Appl. Phys. Lett. **19**, 133104 (2021).

[24] A. M. Goossens, V. E. Calado, A. Barreiro, K. Watanabe, T. Taniguchi, and L. M. K. Vandersypen, Mechanical cleaning of graphene, Appl. Phys. Lett. **100**, 073110 (2012).

[25] M. R. Rosenberger, H.-J. Chuang, K. M. McCreary, A. T. Hanbicki, S. V. Sivaram, and B. T. Jonker, Nano-"squeegee" for the creation of clean 2D material interfaces, ACS Appl. Mater. Interfaces **10**, 10379 (2018).

[26] D. Rhodes, S. H. Chae, R. Ribeiro-Palau, and J. Hone, Disorder in van der Waals heterostructures of 2D materials, Nat. Mater. **18**, 541 (2019).